Automatic Extraction of the Midsagittal Surface from T1-Weighted MR Brain Images Using a Multiscale Filtering Approach

Fernando N. Frascá, Katia M. Poloni, and Ricardo J. Ferrari(✉)

Department of Computing, Federal University of São Carlos,
São Carlos, SP 13565-905, Brazil
rferrari@ufscar.br
https://www.bipgroup.dc.ufscar.br

Abstract. The left and right hemispheres of the human brain are separated by a fissure called interhemispheric (IHF), which is commonly shaped by a geometric plane known as the midsagittal plane (MSP). However, despite the name, the MSP does not always resemble a plan since the brain is not perfectly symmetric. The detection of the MSP in human brain images is an essential task to segment the brain hemispheres. Studies suggest that abnormal values of brain asymmetry may be related to traumas and neurological diseases. Through the years, several computer methods were proposed to detect the MSP automatically. Nonetheless, they constrain the detection to a plane without considering brain asymmetries. In this study, an automatic computer technique is developed to detect a midsagittal surface (MSS) in Magnetic Resonance (MR) images using an MSP as a reference, following by multiscale analysis. Different from the MSP, the MSS follows the natural form of the IHF. The proposed method uses a reference MSP to guide a region of interest that potentially contains the IHF. The 3D MR image is decomposed in 2D slices that are processed, filtered, and piled to form an MSS. The proposed method results have shown an accurate detection in all metrics assessed, i.e., DSC of 0.99 and x-distance of 2.13, and a significant improvement of 2.953 for the x-distance compared with the MSP method.

Keywords: Brain asymmetry · Midsagittal surface · Interhemispheric fissure · Multiscale filter

1 Introduction

Based on the assumption that the human brain exhibits a high level of bi-fold symmetry, one common approach to detect brain pathologies and structural changes in Magnetic Resonance (MR) images is to compare the left and right brain hemispheres in the search for violations of a devised symmetric measure.

© Springer Nature Switzerland AG 2021
O. Gervasi et al. (Eds.): ICCSA 2021, LNCS 12950, pp. 131–146, 2021.
https://doi.org/10.1007/978-3-030-86960-1_10

Several studies have assessed brain asymmetry seeking abnormal asymmetry values due to gender [2,14,23,27,28] and handedness [14,18] differences. These values can also be associated with traumas and neurological diseases, such as schizophrenia [6,9,33], dyslexia [19], autism and developmental language disorder [17], epilepsy [22,30,41], Alzheimer [1,4,5,35,38,39], and Parkinson [31].

In the human brain, the asymmetries are defined based on proportion measures between the brain hemispheres, given that the boundary between each hemisphere is delimited by the interhemispheric fissure (IHF) [15], a deep groove that divides the brain hemispheres in left and right. For quantitative studies, the IHF is represented as a surface that cuts the sagittal axis of the brain, commonly called midsagittal surface (MSS). The precise location of the MSS is an important step in the analysis of neuroimages, and it is of high interest in various medical applications and researches, particularly in studies involving brain pathologies associated with asymmetries. Liu et al. [26] reviewed brain asymmetry analysis methods and their implications to computer-aided diagnosis and reported the importance of the precise identification of the symmetry plane to perform a correct evaluation of hemisphere-wise asymmetries.

Over the last decade, many methods were proposed for brain asymmetries analysis. However, due to the inherent difficulty to precisely detect the IHF, most of them end up handling the MSS as a plane (MSP), which is often considered as a first-order approximation of the MSS [24]. However, the MSP may bias the asymmetry analysis since it may fail to provide a precise representation of the IHF in many cases. Therefore, in this study, we propose a new automatic method to assess brain asymmetries using the MSS detection in T1 weighted (T1-w) MR images of the human brain. The method uses the automatic detected MSP using a previous work developed by our group [11,13] as a starting point for our MSS searching and a 2D multiscale filtering analysis. The aim is to obtain a surface that represents more precisely possible brain asymmetries, overcoming the constraint imposed by other methods presented in the literature, which approximates the IHF as a plane [25].

Our method was evaluated using a set of fifty 2D slices of the axial view of the human brain, extracted from images of three distinct datasets. The automatic MSS projections were compared to manual annotations made by two specialists from the medical field.

The rest of this paper is structured as follows: Sect. 2 provides information about the image dataset used in this study, Sect. 3 present the proposed method and its concepts, Sect. 4 presents the validation metrics, Sect. 5 present the obtained results and Sect. 6 provide the conclusions of this work.

2 Image Datasets

This section presents the datasets used in this study and the set of images used to validate the proposed method. We manually selected thirty-eight MR images from three distinct neuroimaging datasets to include the diversity of the populations on which the method might potentially be deployed, and be certain subjects with brain torque were selected.

We validate our method using manual annotations from two medical doctors (MDs), herein referred to as specialists. We randomly selected fifty 2D slices to validate our experiment results due to manual annotation being an expensive and exhaustive task. The 2D processing occurs after we preprocess the 3D images. Due to the variety of scanners used to acquire the images among databases, all images were resampled to an isotropic resolution of 1 mm.

Neuroimage Analysis Center (NAC): The NAC [16] is a research center affiliated with the Surgical Planning Laboratory and Harvard University. The dataset consists of 149 3-D triangular meshes of distinct brain structures spatially aligned to a T1-weighted (T1-w) image of a healthy 42-year-old male subject and had 1mm isotropic resolution and a matrix size of $256 \times 256 \times 256$ voxels. For this study, we only used the T1-w image as a reference for the preprocessing steps to mitigate problems inherent to image acquisitions and standardize all study images for processing.

Alzheimer's Disease Neuroimaging Initiative (ADNI): The ADNI dataset [21] is part of a project released at the beginning of 2003, idealized by a group of research institutions, private pharmaceutical companies, and non-governmental organizations. The initiative has been looking for ways to determine the progression of Alzheimer's by developing clinical biomarkers for detecting the disease in its early stages. For this study, we used nineteen T1-w MR images of individuals with Alzheimer's disease, from which we randomly selected twenty-two axial slices.

Information eXtraction from Images (IXI): The IXI dataset[1] is developed and maintained by the Neuroimage Analysis Center, from Imperial College London, in the United Kingdom, and it is part of the project Brain Development. Its data are composed of approximately 600 MR brain images acquired with T1-, T2-, and PD-weighting. We used eighteen T1–w RM images of healthy individuals from this dataset, from which we randomly selected twenty-three axial slices.

Simulated Brain Database (BrainWeb): The BrainWeb [3] is a dataset composed of synthetic images of the human brain, provided by the McConnel Brain Imaging Centre, from McGill University, Canada, to help validate research experiments involving MR images of the human brain. We selected only one T1-w MR image of a healthy individual from this dataset, which we randomly selected five axial slices.

3 Methods

This section presents the proposed method for the extraction of the midsagittal surface from T1–w MR brain images.

[1] https://brain-development.org/ixi-dataset/.

3.1 Overview of the Proposed Method

The main idea of the proposed method is to develop a method to detect the MSS that can allow studies to perform a more accurate asymmetry assessment when comparing the brain hemispheres. Our method is composed of three main steps: (a) image preprocessing, (b) IFH sampling, and (c) MSS extraction. Figure 1 presents the general framework of the proposed method.

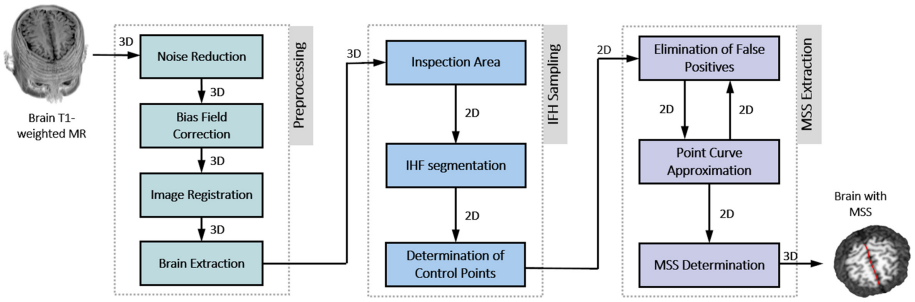


Fig. 1. A schematic block diagram of the proposed method

3.2 Preprocessing

The MR images were first preprocessed for noise reduction using the Non-Local Means algorithm [8] and bias field correction using the N4-ITK technique [40]. This task was performed to minimize the negative effects that noise and bias field may have. Next, image registration was conducted using the Nifty-Reg tool [32] to align all images to the NAC reference image. Finally, brain region extraction was achieved using the Robust Brain Extraction (ROBEX) technique [20] to avoid unnecessary processing.

3.3 IFH Sampling

Following the preprocessing steps, we detected the MSP using the technique proposed in [11,13] and used it as a reference to define the region of interest (ROI) to search for the MSS. Next, we extracted only the even axial slices from the 3D MR images, leading to a set of 128 axial slices. Then, we used the MSP projection for each slice (a straight line) as a reference, herein called midsagittal line (MSL), to define a limiting box (ROI) to search for the MSS, thus avoiding unnecessary processing and minimizing the interference of nearby structures to the MSS. After that, we positioned the limiting box in the longitudinal direction with its sides positioned paralleling and equidistant from the MSL marked on the image slice. Finally, we calculated the length of the limiting box based on the most extreme pixels of the longitudinal axis that presented values of intensity different from zero. Figure 2(a) shows an example of the ROI (rectangle in red colour) overlaid on an axial image slice.

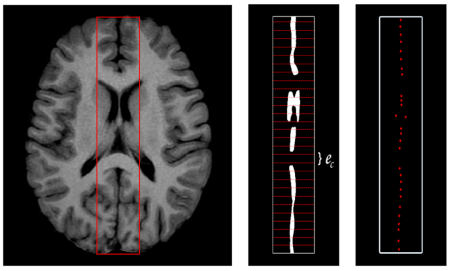


Fig. 2. Example of the ROI (a) delimiting the axial slice, (b) showing the fragmentation lines, and (c) the control points detected

After the ROI demarcation, we enhanced the IHF in each slice image using the multiscale Hessian filter-based technique proposed in [12] for vessel image enhancement. The reason for using this approach is based on the observation that the cerebral sulci, including the IHF, look like a net of curvaceous tubular structures when projected to an axial slice, which may help to identify the MSS 2D projection. The multiscale Hessian filter-based technique works by assessing the relationships between the eigenvalues (λ_1 and λ_2) of a 2×2 Hessian matrix locally created from the neighborhood of each pixel. When visualized on the T1-w MR images, the IHF appears similar to a dark tubular structure (or vessel) on the light background and, according to Table 1 from [12], we have to search for regions in the image where the eigenvalues, λ_1 and λ_2, of the Hessian matrix are low and positive high, respectively to detect tubular structures.

Considering the IHF is naturally connected by other peripheral vessel-like structures, the multiscale Hessian filter-based filtering technique should highlight the IHF sulcus and other undesirable peripheral sulci. To this end, we used morphological operators (erosion and dilation) defined by a thick stick structuring element oriented with its length aligned to the ROI length to eliminate the unwanted structures that mostly manifest in a perpendicular direction to the IHF and are proportionally smaller than it.

Finally, after processing the ROI on the 2D slices to enhance the IHF, we divided the region into equally broad stripes of e_c pixels along the longitudinal axis, as illustrated in Fig. 2(b). Then, we defined the control points (CP) as the centroid point of the IHF fragment present in each stripe, as shown in Fig. 2(c). The stripe widths, e_c, were experimentally defined as 2% of the longitudinal size of the ROI to allow a significant number of CPs to represent the IHF.

Table 1. Possible local patterns that may be detected in an image through analysis of the self-values of the Hessian matrix.

Eigenvalues		Orientation pattern
λ_1	λ_2	
Noise	Noise	Noise, no preferred direction
Low	High−	Tubular structure (bright)
Low	High+	Tubular structure (dark)
High−	High−	Blob-like structure (bright)
High+	High+	Blob-like structure (dark)

3.4 MSS Extraction

After the IHF sampling, we performed a two-step postprocessing. First, we determined the most suitable CPs to build the curve better representing the IHF in each slice and, further, used all IHF curves detected in the 2D planes to create a 3D structure representing the MSS.

The first step was used to eliminate outliers, i.e., control points whose horizontal spatial positions were offset by a certain distance from the reference position defined by the central vertical line of the ROI. To this end, we applied the statistical Z-score test [7] to each test point, with mean and standard deviation parameters estimated from the CP spatial positions. Considering the maximum number of CPs per ROI is lower than 50, we set the Z-score threshold as 2.5 and used it as a criterion for a potential outlier in our experiments , i.e., all points with Z-score value outside the -2.5 and 2.5 range were considered outliers.

The second step used an iterative procedure to remove CP points that may cause disruption in the smoothness of the final reconstructed MSS. This procedure verified if any CP position on the analyzed slice (S_a) was shifted outside a tolerance range (β) when compared to the corresponding point position in a reference slice (S_i). If this happened, then the point was not considered for the construction of the IHF curve. The initial reference slice (S_{i_o}) was defined as the one at the position comprising 40% of the slice sequence, measured from the top to the bottom of the brain. This procedure was based on the observation that the S_{i_o} position in the brain corresponds to the most prominent view of the IHF. The iterative process was performed considering that corresponding points (equal spatial positions) on consecutive slices should not deviate above a tolerance margin; otherwise, they would represent structures with an acute shape, which are unlikely to occur in IHF. At the end of each iteration, the analyzed slice (S_a), with all control points outside the distance tolerance removed, becomes the reference slice (S_i) of the subsequent slice. The value for the tolerance range, β, was experimentally set to 8 pixels.

Finally, we resampled all IHF curves created on each image slice using the B-Spline interpolation [37] to create a new set of control points, each with their respective (x, y) coordinates in the Cartesian plane, and build the 3D structure

of the MSS. We stacked the points so that each point, previously sampled in the (x, y) space, received a new z coordinate, which represented the index of the slice to which that point was associated to build the MSS. We performed this process covering each slice of the image in sequential order and converting the respective points associated with the slice to the 3D plane. At the end of the process, we have a grid of points on the 3D plane representing the MSS.

4 Validation Metrics

We assessed the accuracy of the proposed approach by using empirical discrepancy evaluation methods based on region overlap and average x-distance (in pixels) [34]. The discrepancy was computed between our automatic MSS detection and the two specialists' manual annotations. As mentioned in Sect. 2, we randomly selected fifty 2D slices to validate our experiment results, from which the two MD specialists, abbreviated as specialist 1 (S1) and specialist 2 (S2), have annotated the MSS. They used the Fiji tool [36] with the freehand spline drawing technique to manually annotate the curve that divides the cerebral hemispheres.

Dice Similarity Coefficient (DSC): We used the DSC [10] to evaluate similarity based on the overlap between the masks generated by our detection and the ones of the specialists. The mask images were obtained using the IHF manual annotation and the MSS to define which pixels are belonging to the left and right hemispheres on the ROBEX output mask (i.e., the brain extraction mask). The DSC is calculated as

$$\text{DSC} = \frac{2\,S \cap A|}{|S| + |A|}, \tag{1}$$

where S and A represent the cerebral hemispheres delimiting the masks obtained by the specialist's annotation and by the automatic method, respectively. The DSC values range from 0 to 1, being 1 when there is a complete agreement between the two masks and 0 when there is a complete lack of agreement.

Average x-distance: The x-distance value represents the distance between the curves marked by the automatic method and by a specialist. The measure is an adaptation of the method proposed in [34] and is calculated as

$$x\text{-distance} = \frac{\sum_y (|x^S_{coord} - x^A_{coord}|)}{N}, \tag{2}$$

where x^S_{coord} and x^A_{coord} represent the x coordinate of IHF curve points marked by the specialist and automatic method, respectively, and N is the number of curve points compared along the y axis. Smaller values indicate more proximity between the two curves and larger values otherwise.

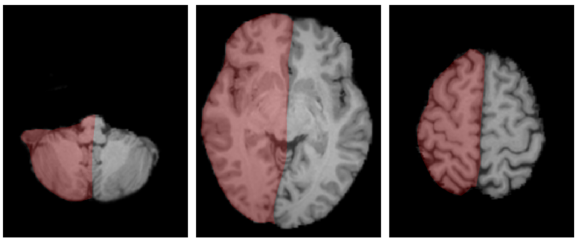
Statistical Analysis: We used the Mann-Whitney U test [29] with the two-tailed hypothesis with a significance level $\alpha = 0.01$ to verify if there were statistically significant differences between the results obtained for the DSC values when

comparing the left and right hemispheres and each specialist annotation with our MSS method. Further, we also verify the average x-distance obtained between each specialist annotation with our MSS method and with a method used as a comparison, the MSP [11,13].

5 Results

The results of the proposed technique for the MSS detection in brain MR images are presented as follows.

DSC Results
Figure 3 shows a visual example of three axial image slices with the MSS delimitation applied to segment the hemispheres. The overlaid red region indicates the left hemisphere and the other the right. From these slices, we can visually notice that the proposed MSS method accurately captured the surface of the hemisphere.



(a) (b) (c)

Fig. 3. Visual example of segmentation of the cerebral hemispheres from automatic delineation.

To ensure we captured the surface accurately, we quantitatively assessed the region overlap results using the DSC. The boxplots in Fig. 4 show the DSC values calculated between the MSS segmentation mask and the two specialists masks, S1 and S2 (considered ground-truths), using three different databases: ADNI, IXI, and BrainWeb. Since we need to separate the left and right hemispheres to generate their masks, we show plots for both hemispheres separately.

For the left hemisphere, we obtained the highest mean DSCs of 0.989 ± 0.005 and 0.989 ± 0.005 for the ADNI dataset when compared with the S1 and S2 specialists, respectively, and for the BrainWeb the corresponding values were 0.989 ± 0.003, and 0.989 ± 0.005. We obtained the smallest interquartile range (IQR) for the ADNI images and the smallest whiskers and number of outliers for the BrainWeb dataset, both compared to the specialist S1. For the IXI dataset, we obtained the lowest mean DSC and the highest IQR, with values of 0.986 ± 0.005 compared with S1 and 0.987 ± 0.003 compared with S2. When tested using

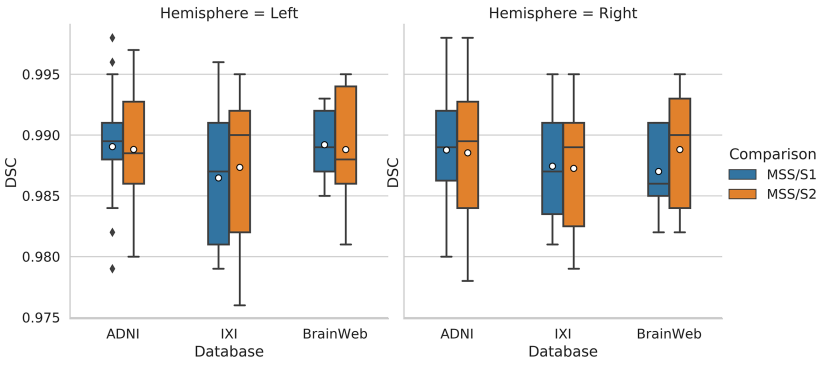


Fig. 4. DSC values for the left and right hemispheres using three different databases: ADNI, IXI, and BrainWeb. S1 and S2 refer to the specialist 1 and 2.

all dataset images, we obtained a mean DSC of 0.988 ± 0.005 and 0.988 ± 0.006, compared with S1 and S2.

For the right hemisphere, we obtained the highest mean DSC of 0.989 ± 0.005 and 0.989 ± 0.006 for the ADNI dataset, a mean DSC of 0.987 ± 0.004 and 0.987 ± 0.004 for the IXI dataset, and 0.987 ± 0.004 and 0.989 ± 0.004 for the BrainWeb, all values compared with S1 and S2, respectively. Using all dataset images, we obtained a mean DSC of 0.988 ± 0.004 compared with S1 and 0.988 ± 0.006 compared with S2.

To assess if the DSC results presented statically significant differences, we performed the Mann-Whitney U test [29]. We compared the left and right hemispheres' DSC results joining and grouping by specialists. Comparing the left and right DSC values, we obtained a p-value of 0.912; while comparing the left and right DSC grouped by specialists, the p-values were 0.438 for the S1 and 0.497 for S2.

We also compared the DSC values for hemisphere and specialists. We obtained a p-value of 0.367 for the comparison between S1 and S2 for the left hemisphere and 0.471 for the right. As it can be noticed, all p-values were bigger than the significance level ($\alpha = 0.01$), meaning that the null test hypothesis was accepted, claiming that both data came from the same distribution. Therefore, we can conclude that despite some minor differences between values, our MSS segmentation obtained similar DSC values for both hemispheres and, more importantly, for the specialist annotations.

Average x-distance

Figure 5 shows a visual example of four distinct axial image slices comparing the MSS application with the two specialists annotations and the MSP proposed in [11,13] as a qualitative assessment.

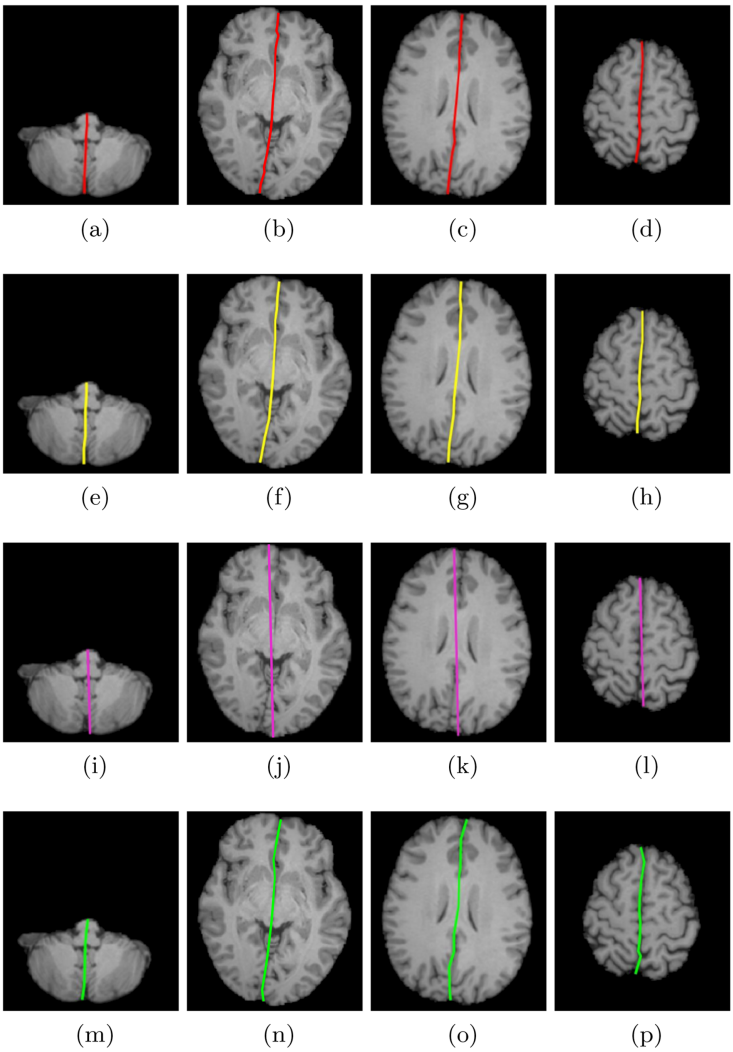


Fig. 5. Example showing four distinct axial slices with (a–d) annotations of the specialist 1 (e–h) annotations of the specialist 2, (i–l) results of the MSP, and (m–p) results of the proposed MSS method.

As it can be noticed, since the MSP assumes that the IHF (midsagittal separation) can be approximated by a plane, it failed the detection in brains with torque, whereas our proposed MSS method successfully captured these changes. We can also notice a very small disagreement between the two specialist's annotations and the MSS method.

The box plots in Fig. 6 and 7 show a comparison of the x-distance between the specialists 1 and 2 (ground-truths) and the MSS detection using three different

databases: ADNI, IXI, and BrainWeb. Further, a comparison was performed between the two specialists' annotations to provide an intra-observer measure, and the MSP detection results were compared with the same ground-truths.

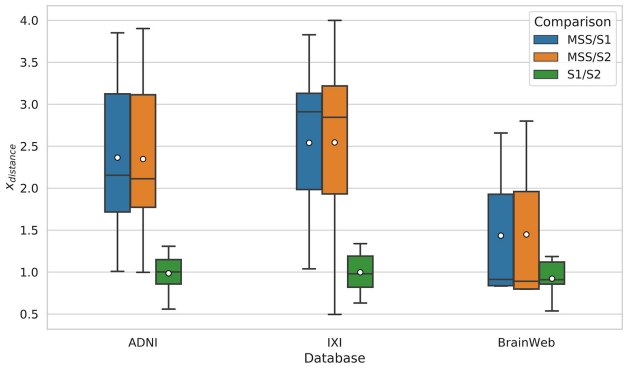


Fig. 6. Boxplot of the x-distance values obtained from the MSS detection compared with specialist 1 (MSS/S1) and specialist 2 (MSS/S2) and the two specialists annotations (S1/S2) compared using three different databases: ADNI, IXI, and BrainWeb.

To better understand the results and show that our results were compared with consistent annotations, Fig. 6 provides a quantitative assessment of the specialists' annotations in the boxplots of green color (S1/S2). Based on the small IQR values between the annotations, we can state that the specialists have a high degree of agreement, with a mean x-distance of 0.985 ± 0.207 for the ADNI slices, 0.998 ± 0.21 for the IXI slices, and 0.922 ± 0.256 for the BrainWeb slices, allowing an overall mean value of 0.968 ± 0.224.

When assessing our MSS detection, by comparing it with S1 and S2 annotations, we achieved mean x-distance results of 2.364 ± 0.897 and 2.347 ± 0.908 for the ADNI, with the highest IQR values in both comparisons. For the IXI, we achieved the highest mean x-distance values, with 2.54 ± 0.853 and 2.544 ± 0.93, and also the minimum and maximum distances. Finally, for the BrainWeb, we obtained the lowest value of mean x-distance values, with 1.434 ± 0.862 and 1.449 ± 0.9 and with the smallest IQR values. The assessment using all image datasets showed mean x-distance values of 2.113 ± 0.913 and 2.113 ± 0.913 compared with the specialists 1 with 2, respectively.

As shown in the box plots in Fig. 7, comparison between the MSP method with S1 and S2 using the ADNI images showed a mean x-distance result of 6.144 ± 1.779 for the specialist S1 and 6.133 ± 1.796 for S2. The same experiment with the IXI images resulted in mean x-distance results of 6.429 ± 2.815 and 6.431 ± 2.766 for the specialists S1 and S2. The same analysis using images from the Brain Web dataset showed mean x-distance values of 2.626 ± 1.225 and 2.604 ± 1.226 for the specialists 1 and 2, respectively. The highest whisker

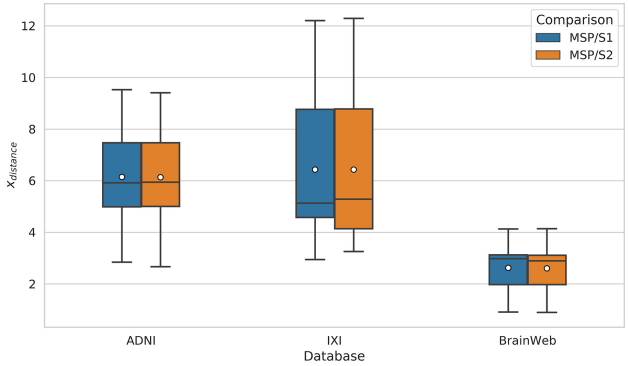


Fig. 7. Boxplot of the x-distance values obtained from the MSP detection compared with specialist 1 (MSP/S1) and specialist 2 (MSP/S2) compared using three different databases: ADNI, IXI, and BrainWeb.

values were noticed for the IXI dataset. The assessment using all image datasets showed a mean with values of 5.066 ± 1.94 for S1 and 5.056 ± 1.929 for S2.

We also used the Mann-Whitney U test [29] to check if there are statically significant differences for the x-distance results obtained by comparing the MSS and MSP methods with S1 and S2. First, we compared the x-distance results for the MSS method with S1 and S2 specialists and obtained a p-value of 0.466, meaning that the test failed to reject H0 and there are no significant differences between the two distributions. Therefore, despite some differences between the specialist's annotations, our method has shown consistent results with both. Next, joining the specialists, we compared the results of our method with the MSP and obtained a p-value of 3.117e–16. After that, grouping by specialists, we repeated the previous experiment and obtained p-values of 1.22e–13 for S1 and 2.937e–14 for S2. Considering the p-value results and the significance level of 0.01, we can discard the null test hypothesis (H0) and conclude that the results compared with the MSP are statistically distinct and do not come from the same population.

For the final analysis, we evaluated the MSS performance using images with curved FIH, i.e., high brain torque. Both specialists manually labeled the images according to two categories: visible torque and non-visible torque. The term brain torque refers to the opposite asymmetry of brain regions. The results are shown in Table 2. For comparison purposes, the results of applying the MSP method [11,13] are also shown. With these results, we noticed that our method is more robust in capturing correctly different brain torques. We obtained similar values for the two categories, i.e., visible torque and non-visible torque, compared to the two specialists. In contrast, when analyzing the MSP results, we noticed that the method was not able to capture the brain torques, which resulted in differences of about 3.5 in the x-distance between the two categories. Furthermore, our results were more accurate than the MSP even when comparing brains with visible torque.

Table 2. Result of the x-distance grouped by category

	x-distance			
	MSS/S1	MSS/S2	MSP/S1	MSP/S2
Visible torque	2.36 ± 0.70	2.37 ± 0.73	7.48 ± 2.09	7.48 ± 2.0
Non-visible torque	2.34 ± 1.103	2.32 ± 1.16	3.94 ± 1.18	3.93 ± 1.15

6 Conclusions

Segmentation of brain hemispheres is widely used to assess brain asymmetries and their implications to computer-aided diagnosis. Most studies have focused on identifying a plane to represent the interhemispheric fissure that divides both hemispheres. However, a plane cannot truly represent the fissure when working with brains presenting torque. According to Toga et al. [39], brain asymmetry levels vary with aging, gender and handedness differences, and the development of diseases. Some diseases, such as Alzheimer's, progress asymmetrically, increasing the brain torque. Therefore, to overcome this limitation, we developed a method to obtain the surface that can precisely represent the interhemispheric fissure, dealing with torque and, consequently, capturing brain asymmetries.

We assess our results using fifty axial slices from T1–w MR brain images, in which two domain specialists manually annotated to use as ground-truths. Our method achieved an accurate detection in quantitative metrics, with a DSC of 0.99 and x-distance of 2.13. We also compared the specialists' annotations distances and verified that the ground-truths have a high degree of agreement. Furthermore, we compared our results with the MSP method [11,13] and achieved x-distance values with a difference of 2.95 between the methods. Lastly, we contrast the method results in brains with different torque degrees and verify the stability of our method to torque.

Acknowledgment. Funding for ADNI can be found at http://adni.loni.usc.edu/about/#fund-container.

Funding Statement. This study was financed by the Fundação de Amparo à Pesquisa do Estado de São Paulo (FAPESP) (grant numbers 2018/08826-9 and 2018/06049-5).

References

1. Ardekani, B.A., Hadid, S.A., Blessing, E., Bachman, A.H.: Sexual dimorphism and hemispheric asymmetry of hippocampal volumetric integrity in normal aging and Alzheimer disease. Am. J. Neuroradiol. **40**(2), 276–282 (2019)
2. Ashburner, J., Hutton, C., Frackowiak, R., Johnsrude, I., Price, C., Friston, K.: Identifying global anatomical differences: deformation-based morphometry. Hum. Brain Mapp. **6**(5–6), 348–357 (1998)

3. Aubert-Broche, B., Griffin, M., Pike, G.B., Evans, A.C., Collins, D.L.: Twenty new digital brain phantoms for creation of validation image data bases. IEEE Trans. Med. Imaging **25**(11), 1410–1416 (2006)
4. Barbará-Morales, E., Pérez-González, J., Rojas-Saavedra, K.C., Medina-Bañuelos, V.: Evaluation of brain tortuosity measurement for the automatic multimodal classification of subjects with Alzheimer's disease. Comput. Intell. Neurosci. **2020**, 11 (2020)
5. Barnes, J., Scahill, R.I., Schott, J.M., Frost, C., Rossor, M.N., Fox, N.C.: Does Alzheimer's disease affect hippocampal asymmetry? Evidence from a cross-sectional and longitudinal volumetric MRI study. Dement. Geriatr. Cogn. Disord. **19**(5–6), 338–344 (2005)
6. Bartko, J.J.: Measurement and reliability: statistical thinking considerations. Schizophr. Bull. **17**(3), 483–489 (1991)
7. Brase, C.H., Brase, C.P.: Understanding Basic Statistics. Nelson Education, Toronto (2013)
8. Buades, A., Coll, B., Morel, J.M.: A review of image denoising algorithms, with a new one. Multiscale Model. Simul. **4**(2), 490–530 (2005)
9. Crow, T.J.: Schizophrenia as an anomaly of cerebral asymmetry. In: Imaging of the Brain in Psychiatry and Related Fields, pp. 3–17. Springer International Publishing, Heidelberg (1993). https://doi.org/10.1007/978-3-642-77087-6_1
10. Dice, L.R.: Measures of the amount of ecologic association between species. Ecology **26**(3), 297–302 (1945)
11. Ferrari, R.J., Villa-Pinto, C.H., Moreira, C.A.F.: Detection of the midsagittal plane in MR images using a sheetness measure from Eigen analysis of local 3D phase congruency responses. In: International Conference on Image Processing (ICIP), pp. 2335–2339. IEEE, Phoeniz, Arizona (2016)
12. Frangi, A.F., Niessen, W.J., Vincken, K.L., Viergever, M.A.: Multiscale vessel enhancement filtering. In: Wells, W.M., Colchester, A., Delp, S. (eds.) MICCAI 1998. LNCS, vol. 1496, pp. 130–137. Springer, Heidelberg (1998). https://doi.org/10.1007/BFb0056195
13. de Lima Freire, P.G., Gregório da Silva, B.C., Villa Pinto, C.H., Ferri Moreira, C.A., Ferrari, R.J.: Midsaggital plane detection in magnetic resonance images using phase congruency, hessian matrix and symmetry information: a comparative study. In: Gervasi, O., et al. (eds.) ICCSA 2018. LNCS, vol. 10960, pp. 245–260. Springer, Cham (2018). https://doi.org/10.1007/978-3-319-95162-1_17
14. Good, C.D., Johnsrude, I., Ashburner, J., Henson, R.N., Friston, K.J., Frackowiak, R.S.: Cerebral asymmetry and the effects of sex and handedness on brain structure: a voxel-based morphometric analysis of 465 normal adult human brains. Neuroimage **14**(3), 685–700 (2001)
15. Guillemaud, R., Marais, P., Zisserman, A., McDonald, B., Crow, T.J., Brady, M.: A three dimensional mid sagittal plane for brain asymmetry measurement. Schizophr. Res. **2**(18), 183–184 (1996)
16. Halle, M., et al.: Multi-modality MRI-based atlas of the brain. http://www.spl.harvard.edu/publications/item/view/2037 (2017)
17. Herbert, M.R., et al.: Brain asymmetries in autism and developmental language disorder: a nested whole-brain analysis. Brain **128**(1), 213–226 (2005)
18. Hervé, P.Y., Crivello, F., Perchey, G., Mazoyer, B., Tzourio-Mazoyer, N.: Handedness and cerebral anatomical asymmetries in young adult males. Neuroimage **29**(4), 1066–1079 (2006)

19. Hynd, G.W., Semrud-Clikeman, M., Lorys, A.R., Novey, E.S., Eliopulos, D.: Brain morphology in developmental dyslexia and attention deficit disorder/hyperactivity. Arch. Neurol. **47**(8), 919–926 (1990)
20. Iglesias, J.E., Liu, C.Y., Thompson, P.M., Tu, Z.: Robust brain extraction across datasets and comparison with publicly available methods. IEEE Trans. Med. Imaging **30**(9), 1617–1634 (2011)
21. Jack, C.R.J., et al.: The Alzheimer's disease neuroimaging initiative (ADNI): MRI methods. J. Magn. Reson. Imaging **27**(4), 685–691 (2017)
22. Kim, J.S., Koo, D.L., Joo, E.Y., Kim, S.T., Seo, D.W., Hong, S.B.: Asymmetric gray matter volume changes associated with epilepsy duration and seizure frequency in temporal-lobe-epilepsy patients with favorable surgical outcome. J. Clin. Neurol. (Seoul, Korea) **12**(3), 323 (2016)
23. Kovalev, V.A., Kruggel, F., von Cramon, D.Y.: Structural brain asymmetry as revealed by 3D texture analysis of anatomical MR images. In: Object Recognition Supported by User Interaction for Service Robots, pp. 808–811. IEEE, Quebec, Canada (2002)
24. Kruggel, F., von Cramon, D.Y.: Alignment of magnetic-resonance brain datasets with the stereotactical coordinate system. Med. Image Anal. **3**(2), 175–185 (1999)
25. Kuijf, H.J., Van Veluw, S.J., Geerlings, M.I., Viergever, M.A., Biessels, G.J., Vincken, K.L.: Automatic extraction of the midsagittal surface from brain MR images using the Kullback-Leibler measure. Neuroinformatics **12**(3), 395–403 (2014)
26. Liu, S.X.: Symmetry and asymmetry analysis and its implications to computer-aided diagnosis: a review of the literature. J. Biomed. Inform. **42**(6), 1056–1064 (2009)
27. Lucarelli, R.T., et al.: MR imaging of hippocampal asymmetry at 3T in a multiethnic, population-based sample: results from the Dallas Heart Study. Am. J. Neuroradiol. **34**(4), 752–757 (2013)
28. Luders, E., Gaser, C., Jancke, L., Schlaug, G.: A voxel-based approach to gray matter asymmetries. Neuroimage **22**(2), 656–664 (2004)
29. Mann, H.B., Whitney, D.R.: On a test of whether one of two random variables is stochastically larger than the other. Ann. Math. Statist. **18**(1), 50–60 (1947)
30. Martins, S.B., Benato, B.C., Silva, B.F., Yasuda, C.L., Falcão, A.X.: Modeling normal brain asymmetry in MR images applied to anomaly detection without segmentation and data annotation. In: Medical Imaging 2019: Computer-Aided Diagnosis, vol. 10950, p. 109500C. SPIE, San Diego, California (2019)
31. Ortiz, A., Munilla, J., Martínez, M., Gorriz, J.M., Ramírez, J., Salas-Gonzalez, D.: Parkinson's disease detection using Isosurfaces-based features and Convolutional Neural Networks. Front. Neuroinform. **13**(48), 48 (2019)
32. Ourselin, S., Stefanescu, R., Pennec, X.: Robust registration of multi-modal images: towards real-time clinical applications. In: Dohi, T., Kikinis, R. (eds.) MICCAI 2002. LNCS, vol. 2489, pp. 140–147. Springer, Heidelberg (2002). https://doi.org/10.1007/3-540-45787-9_18
33. Ribolsi, M., Daskalakis, Z.J., Siracusano, A., Koch, G.: Abnormal asymmetry of brain connectivity in schizophrenia. Front. Hum. Neurosci. **8**, 1010 (2014)
34. Ruppert, G.C.S., Teverovskiy, L., Yu, C.P., Falcao, A.X., Liu, Y.: A new symmetry-based method for mid-sagittal plane extraction in neuroimages. In: International Symposium on Biomedical Imaging: From Nano to Macro, pp. 285–288. IEEE, Chicago, Illinois, USA (2011)

35. Sarica, A., et al.: MRI asymmetry index of hippocampal subfields increases through the continuum from the mild cognitive impairment to the Alzheimer's disease. Front. Neurosci. **12**(576), 1–12 (2018)
36. Schindelin, J., et al.: Fiji: an open-source platform for biological-image analysis. Nat. Methods **9**(7), 676–682 (2012)
37. Späth, H.: One Dimensional Spline Interpolation Algorithms. CRC Press, Boca Raton (1995)
38. Thompson, P.M., et al.: Dynamics of gray matter loss in Alzheimer's disease. J. Neurosci. **23**(3), 994–1005 (2003)
39. Toga, A.W., Thompson, P.M.: Mapping brain asymmetry. Nat. Rev. Neurosci. **4**(1), 37–48 (2003)
40. Tustison, N.J., et al.: N4ITK: improved N3 bias correction. IEEE Trans. Med. Imaging **29**(6), 1310–1320 (2010)
41. Wu, W.C., et al.: Hippocampal alterations in children with temporal lobe epilepsy with or without a history of febrile convulsions: evaluations with MR volumetry and proton MR spectroscopy. Am. J. Neuroradiol. **26**(5), 1270–1275 (2005)